IEEE Access
Multidisciplinary | Rapid Review | Open Access Journal

Received October 15, 2020, accepted October 28, 2020, date of publication November 6, 2020, date of current version November 18, 2020.

*Digital Object Identifier 10.1109/ACCESS.2020.3036373*

# Efficient Energy Conversion in Electrically Assisted Bicycles Using a Switched Reluctance Machine Under Torque Control

**BAHAREH ZAGHARI[1], (Member, IEEE), ALEKSAS STUIKYS[2], ALEX S. WEDDELL[1], (Member, IEEE), AND STEVE BEEBY[1], (Senior Member, IEEE)**
[1]School of Electronics and Computer Science, University of Southampton, Southampton SO17 1BJ, U.K.
[2]RETORQ Motors Ltd., London N1 7GU, U.K.

Corresponding author: Bahareh Zaghari (bahareh.zaghari@soton.ac.uk)

This work was supported by the U.K. Engineering and Physical Sciences Research Council (EPSRC) under Grant EP/P010164/1.

**ABSTRACT** The prospect of physical exertion commonly acts as a deterrent to the adoption of cycling for everyday transport. A battery powered assistance torque electric motor could alleviate such physical exertion by reducing the effort required by the cyclist. This study investigates the potential effectiveness, efficiency, and energy saving of electrically-assisted cycling when assistance torque of a switched reluctance motor is designed to vary in accord to the cyclist instantaneous torque at the pedal cranks. Specifically, the modulated motor assistance torque is delivered at the least efficient human input torque points on the cycle. For a representative short distance cycling schedule modulating the instantaneous torque of the on-board electric motor causes the electric energy expenditure to not exceed that of the assisted cycling mode of an identical constant-torque motor. Furthermore, for the same speed profile cycling journey with added road gradient and head wind resistance, the energy expenditure of the modulated torque motor is equal to the constant torque motor. These findings indicate significant improvements in the cycling experience.

**INDEX TERMS** Modulated cycling torque, energy conversion, electric bike, switched reluctance machine, battery.

## I. INTRODUCTION

Electrically assisted bicycles (e-bikes) require pedaling, and permit the rider to switch on battery-powered motor to reduce pedaling effort. In general, the motor assistance stops when the rider stops pedaling or when the bicycle exceeds specified speed thresholds. E-bikes require less physical exertion and enable easier cycling on up-hill cycling routes. This design is thought to encourage more people to adopt cycling as a means of transportation. The results from a trial in Brighton, UK, where 80 employees were given an e-bike six to eight used them at least once a week. This resulted in an average reduction of 20% in car mileage [1]. The results of this study motivate the adoption of electrically-assisted bicycles with on-board battery powered motors. Commercial e-bikes are generally heavier than conventional bicycles due to the additional battery, however the motor in these bikes is engaged by pedaling, and the level of assistive power given by the motor can be adjusted (also supporting E-bikes motor-only mode). In this article, we present an e-bike (with mid-motor) that reduces energy usage and as a result presents potential for downsized electric powertrain to improve the cycling experience.

In previous research studies brushless DC (BLDC) machines [2], [3], permanent magnet synchronous machines [4], different geared brushless-DC motor drives [5], Switched Reluctance (SR) machines [6], permanent magnet flux switching machines [7], synchronous reluctance motors [8], and five-phase outer-rotor interior permanent magnet motors [9] have been considered for use in e-bikes.

Conventional e-bikes are designed with Brushless DC (BLDC) motors because of their reliability, power density, and small form factor [10]. Other e-bike motors, such as Induction Machines (IM), have a lower torque density and power efficiency in comparison with BLDC motors [11]. Switched Reluctance Motors (SRMs) can have sensorless control and are light, rugged, and low cost, but they run more loudly than BLDC motors [12]. SRMs have no cogging

The associate editor coordinating the review of this manuscript and approving it for publication was Giambattista Gruosso.

torque, and therefore do not affect cycling when there is no energy input to the motor (e.g. when battery is low), unlike motors with permanent magnets. Brushed and brushless DC permanent magnet motors have higher cost due to the cost of the permanent magnets. SR machines have a simple structure with high torque and power density, however they require a complex control system [13], [[14]. BLDC machines have higher torque ripples, however for e-bikes with a large mass inertia and high gearing ratios (acting as dampers to the pulsating torque) this is not concerning. SRMs have been studied as an alternative cheaper motor in e-bikes [6], [15]–[17]. Most of these studies have focused on optimizing the SRM design for maximum output torque, output power and efficiency [15]–[18]. When the outer diameter of an e-bike motor is kept as a fixed parameter, and the SRM is optimized for its weight, it is shown that the BLDC motor has higher efficiency than SRM [16]. SRMs have potential to reach similar efficiency as permanent magnet machines if the motor topology is carefully designed [12], [18], [19]. Synchronous Reluctance Machines (SynRM) with a segmented rotor topology have high torque, efficiency, and power range in comparison with Interior Permanent Magnet Switched Reluctance (IPMSR) machines [18]. Outer Segmental Rotor Synchronous Reluctance motors (OSRSyncRMs) for e-bikes have a higher average torque than (SynRM) due to reduction in flux path and flux leakage [18]. Mutually coupled SRM (MCSRM) has potential to produce higher torque at low speed, though the torque performance is shown to be inferior to both the non-coupled SRM and permanent magnet synchronous motor at high speed [20].

In this article we introduce a SRM torque controlled by the time-varying torque generated by the cyclist. This torque is expected to improve the overall efficiency and reduce cycling effort. Different torque control methods have been addressed in literature. The examples are direct average torque control, current profiling through torque sharing functions, direct torque control, and direct instantaneous torque control. The average torque control is applied by maintaining the driving angles while varying the electric current reference in each cycle or when the electric current and the driving angles are controlled [21]. Most studies focus on methods that enable real time variation of all control variables. This can be achieved online, through formulation and controllers or through genetic algorithms, or it can be achieved offline, using lookup tables. Accurately calculating torque is an important part of the torque control in nonlinear electrical machines. In [22] instantaneous electromagnetic torque waveforms of the SR machines are calculated based on a simple vector analysis of the flux-linkage map to avoid integration, non-linear curve fitting or geometrical series summation.

The novelty of this investigation is in the idea of providing motor assistance during the instantaneous human torque fluctuations within one crank revolution, rather than providing the constant torque assistance as with traditional e-bikes. The contributions of this work are: (a) Human torque is considered as part of the SRM design process to reduce the effort that the cyclist needs to put into cycling. This will achieve better performance and lower energy consumption. (b) The motor can work under torque modulation as well as being dual mode. The first operating mode is when the SR machine acts as a motor with a sinusoidally varying torque to provide pedaling assistance to the cyclist. The second operating mode is when the SR machine acts as an energy harvester to recuperate and store energy which is otherwise wasted. The first operating mode is investigated in this article. A like-for-like comparison is performed for the modulated and constant assistive motoring torque modes in order to demonstrate the advantages the modulated assistive mode can offer.

## II. ANALYZING HUMAN CYCLING

### A. INEFFICIENCIES IN HUMAN CYCLING

Torque produced by a human at the pedal cranks of a bicycle varies through the complete crank revolution [23]–[29]. The pedaling torque peaks and troughs reach maximum and minimum value at particular crank angles. Thus produced human cycling torque is of lesser concern when cycling at a steady speed or even while modestly accelerating along a level road [27], but becomes significantly less effective when cycling up along a steep hill [26] when the cycling effort and therefore the cyclist energy expenditure becomes considerable [28]. Similar difficulties are observed when starting to cycle from a complete standstill, which cyclists compensate for by using a lower gear to increase torque. This cycling difficulty is exacerbated by the uneven production of torque by the cyclist, which cannot be smoothed completely by cyclist effort or cycling techniques alone [27]–[29]. Another difficulty caused by this uneven cycling torque is that energy is not efficiently expended by the cyclist. The cycling effectiveness (for both legs simultaneously) can be readily modelled as [23]

$$\eta\left(\theta_1\right) = \left(\frac{T\left(\theta_1\right)/L_{ca}}{\sqrt{F_H^2 + F_V^2}}\right)(\%)\,, \tag{1}$$

where $T(\theta_1)$ is the torque at a chosen crank angle, $L_{\mathrm{ca}}$ is the crank arm length, $F_{\mathrm{H}}$ is the forward (horizontal) force exerted by the foot, and $F_{\mathrm{V}}$ is the downward (vertical) force exerted by the foot whilst pedaling.

Fig. 1 shows how this cycling effectiveness varies as a function of the crank angle. Fig. 1 indicates that, since both legs are used simultaneously, there are two peaks in the complete pedal crank revolution and therefore the braking torque of the trailing foot in the upstroke region is compensated by the down stroke of the leading foot. However, the algebraic difference between the total input cycling effort (the denominator of Eq. (1)) and the effective output cycling propulsion force (the numerator of Eq. (1)) at any given pedal crank angle is significant, limiting cycling force effectiveness below 60% at the most effective pedal crank positions. On average, the cycling effectiveness is less than 50% if taken over the complete crank revolution.

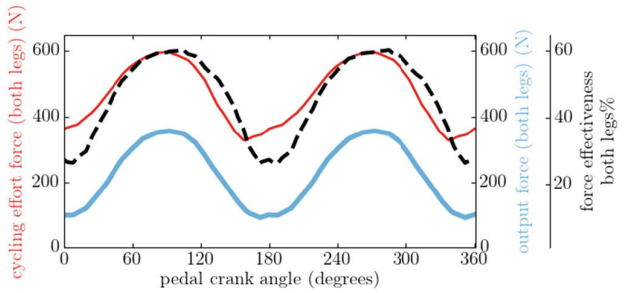


**FIGURE 1.** Human cycling effectiveness at 82 (cranks per minute) for both legs. Crank arm length taken as 0.19 (m). Data adopted from [26].

### B. EFFICIENT ASSISTIVE HUMAN-ELECTRIC CYCLING

The preceding analysis confirms that the conventional bicycle pedal crank mechanism is ineffective for the human pedaling force conversion into propulsive force of the bicycle. To aid the cycling effort bicycle manufacturers have resorted to the electrification solution whereby an electric motor and an electrical energy source for it are fitted onboard the bicycle [30]. This is beneficial from the cycling effort point of view since the electric motor is used to deliver a proportion of the cycling torque which can exceed that of the human [31], [32].

Fig. 2 shows the effects of the two alternative assistive motor torque modes (with a gearing ratio of 10) in addition to the human cycling torque, using the model introduced in Eq. 1. In the case of the conventional e-bikes, the constant motor torque (motor 1) is delivered to the pedal cranks or directly into the bicycle wheel thus reducing the human input torque required to maintain the same crank rate (''seated hill'' reduced effort in Fig. 2a). In Fig. 2a, total propulsion torque is the sum of the instantaneous human and the motor contributions.

Fig. 2a shows that the added constant motor torque does not in itself increase the human cycling effectiveness, since the human output torque is still sinusoidal, and the cycling effectiveness, as given by Eq. (1) and seen in Fig. 1, will remain below 50% on average. Therefore, the cycling effectiveness and the ease of cycling are different considerations. Human cycling effort is concerned with the comfort, whereas the cycling effectiveness is concerned with the effective energy expenditure. This investigation is concerned with the method of decreasing human cycling effort to an acceptable comfort level while maintaining or significantly improving the cycling effectiveness.

We propose to combine such produced sinusoidal human torque with the onboard electric motor torque of the same characteristic shape and magnitude, albeit offset from the human torque by 90 degrees of the pedal crank angle as shown in Fig. 2b. This approach does not aid the human torque when the cycling effectiveness and the torque magnitudes are at the highest level. Since the motor torque can be modulated throughout the complete crank revolution, the total cycling effort of the human (sinusoidal reduced effort) and the motor (motor 2) is equal to the previously considered

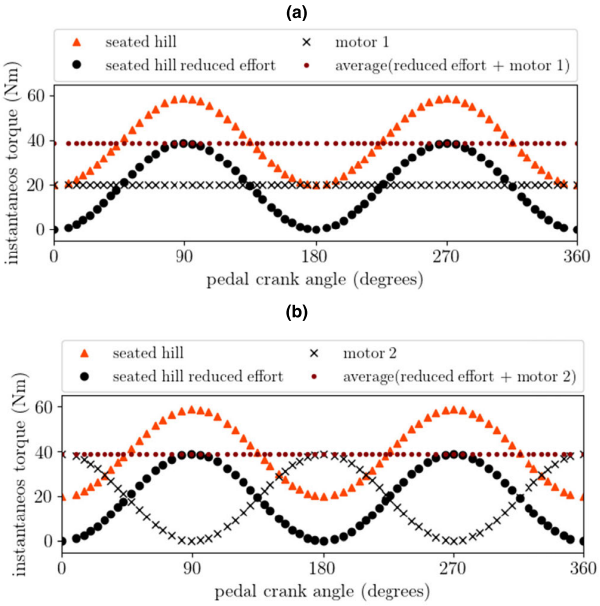


**FIGURE 2.** (a) Instantaneous cycling torque and constant motor (motor 1) assistive torque. (b) Instantaneous cycling torque and time varying motor (motor 2) assistive torque.

case of constant motor torque input (motor 1) and the human reduced effort as in Fig. 2a. The twofold benefit of the proposed torque control method is that the human efficiency is fully utilized while effectiveness has increased at the specific low efficiency crank angles (Fig. 1). This can be potentially achieved while the size of the motor with a modulated torque is smaller than the motor that delivers the constant torque (motor 1) throughout the complete crank revolution due to change in duty cycle. Consequently the machine can be smaller than the equivalent constant torque machine, since cooling requirements are lower. Therefore, the onboard electric motor size and cost is lower compared to the constant torque case, which requires a smaller onboard energy storage device (e.g. a battery), resulting in lowered cost and reduced weight. It is further assumed that since the human torque can be expressed as

$$T = f\left(\sin(\theta)\right), \tag{2}$$

and provided that this torque is varied over the complete pedal crank revolution $0 \leq \theta \leq 2\pi$, the average human torque is

$$T_{\text{av}} = \frac{1}{2\pi}\int_{0}^{2\pi} f(\sin(\theta))\mathrm{d}\theta. \tag{3}$$

From Eq. 3 it is seen that the same average torque value will be obtained for the modulated motor torque profile in Fig. 2b, since this curve is of the exact shape to the human torque profile offset by 90 degrees in phase. Eq. (3) shows that constant and modulated motor torque will be equal, so the cyclist will be indifferent as to the assistance torque profile.

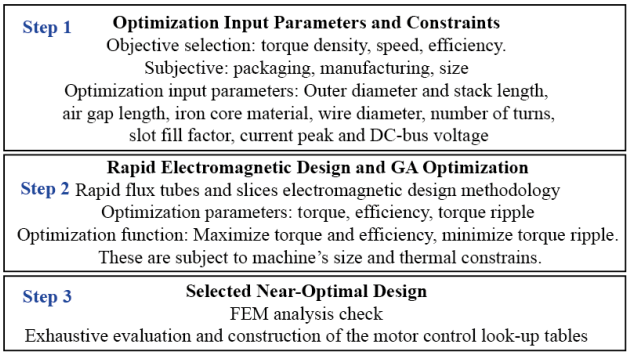


**FIGURE 3.** SR machine selection, electromagnetic design and optimization steps for the electrically assisted bicycle propulsion application.

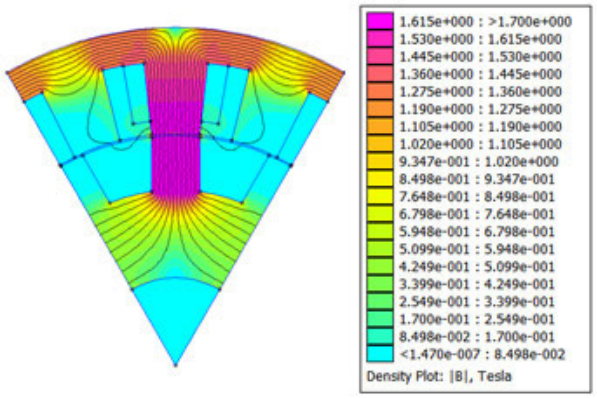


**FIGURE 4.** Flux density at the pole when the maximum current is applied. This result is obtained using FEMM [36].

## III. ELECTROMAGNETIC DESIGN AND OPTIMIZATION OF THE SRM

The compelling benefits of the modulated torque from an onboard electric motor require a capable electric machine technology. Many electric machine technologies can be utilized [3], [5]; however, achieving a low cost and simple manufacturing process suggests SR machine technology as a suitable choice. Previous investigations [6] and successful commercial examples (e.g. SR Drives Ltd.) indicate that SR machines provide a low cost alternative for the high-volume electric bicycle propulsion application. Following the steps in Fig. 3, 18 stator/12 rotor three phase SR machine was selected due to the torque dense topology of this geometrical arrangement [33]. This configuration generates 36 torque pulses per each revolution of the SR motor rotor, as given by

$$S = mN_r, \tag{4}$$

where $S$ is the number of strokes per revolution, $m$ is the number of phases and $N_r$ is the number of the rotor poles [14].

The methods presented in [34] have been adopted to find the best SR machine geometry for this application. The main operating parameters of the proposed SR machine are given in Table 1.

**TABLE 1.** 18/12 Three phase SR machine parameters.

| Design Parameters | SRM/G |
|---|---|
| Outer diameter and stack length [mm] | 100 and 80 |
| Air gap length [mm] | 0.3 |
| Iron core material | M19-0.35mm |
| Wire diameter [mm] | 1.0 |
| Number of turns [turns] | 16 |
| Slot fill factor [%] | 57 |
| Current, peak [A] | 30 |
| DC-bus voltage [V] | 45 |
| RMS current (at 1200rpm) [Arms] | 20 |
| Max Torque (at 1200rpm) [Nm] | 3 |
| Max Torque (at 600rpm) [Nm] | 6 6.0 |

The selection, design and optimization tasks for the chosen SR machine technology were implemented with a multitude of electromagnetic analysis and design techniques, including the rapid flux tubes and slices technique [34], Genetic Algorithm (GA) based optimization and a finite element method implementation from the MagNet numerical simulation software [35]. A simplified flow diagram of the performed optimization processes is presented in Fig. 3, from our previous investigations in [34]. The main aim of this investigation is to perform a like-for-like comparison of the torque control strategy, and to investigate if the energy savings of the electrically assisted bicycle with the sinusoidally varying assistive torque mode can be made. Therefore, the same SR machine design was used in the comparisons. Furthermore, no attempt was made to design a particular bicycle (or the SRM mechanical mounting position) being specified; instead it was assumed that the SRM can be arranged as required provided the specified gearing ratio between the motor and the bicycle crank case is realized.

After selecting the SR machine topology, the electromagnetic optimization is performed for the specified size and operating constraints (Table 1). The GA based optimization [34] is used to search for the optimal SR machine design from the large number of generated candidate solutions. The criterion of the selection of the "best" design from this list of candidates is: at least one of the optimization objectives of the best candidate design has to be better than for the rest of the candidates, and the rest of the objectives of the best candidate design are not worse from amongst all of the other candidates. The selected optimal design is subsequently checked for accuracy with finite element analysis and, if such design is found to be accurate, it is chosen as the SR machine design for which the extraction of control look-up tables is performed. Figure 4 shows the flux density at the poles of the designed SR machine at the maximum phase current.

Figure 5 shows the rapid flux-tubes and MagNet generated results comparison of the flux-linkage curves for the aligned and the unaligned rotor position of the chosen SR machine design. The chosen SR machine peak phase current specified in Table 1 is 30 (A) and therefore the peak current in the model was extended beyond this value in Fig. 5 to check if

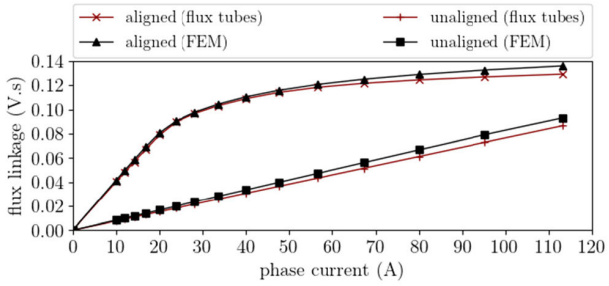


**FIGURE 5.** Flux-linkage versus phase current for aligned and unaligned positions of the designed 18/12 SR motor.

the performed rapid flux-tubes optimization method [34] is sufficiently accurate beyond the normal operating limits of the SR machine. Also, the RMS current of 20 A corresponding to a particular speed in Table 1 does not equal to the static phase current in Fig. 5.

The comparison in Fig. 5 shows that the agreement between the two methods is close. By maximizing the area bounded by the aligned and the unaligned flux-linkage curves in Fig. 5 the torque is obtained as [14]

$$T = \frac{m \cdot N_r . W}{2\pi}, \tag{5}$$

where $W$ is the area bounded by the aligned and the unaligned flux-linkage curves and is measured in units of joule.

The completed design optimization of the SR machine enabled the construction of the turn-on and turn-off angle control look-up tables, as in Fig. 6a and 6b both represented together with the selected constant power curves to be determined together with the efficiency in Fig. 6c, as well as phase current peak and torque ripple maps. The SR machine efficiency in Fig. 6c has been calculated accounting for copper losses, the iron losses, and the mechanical losses. The resistance is R = 0.4971 Ohm for each phase for calculation of copper losses.

The control look-up tables and the efficiency map were subsequently used for the dynamic simulation of the required assistive modulated motor torque for the SRM control scheme shown in Fig. 7. Figure 7 also shows that the look-up tables form a critical part of the dynamic control of the SRM torque, since the demanded torque signal is matched to the stored turn-on and turn-off angles at which the SRM's half-bridge converter is used to switch the phase current for each of the machine phases. The torque demand signal $T_{\text{demand}}$ can be generated in a number of ways depending on the cost and flexibility of the operation. In Fig. 7 two optional alternatives are shown any of which, or both, can be used to generate the torque demand signal including the torque signal generated from a torque sensor or manually set assistance signal. Once the torque signal is read by the SRM controller together with the rotor position signal these signals are then used to retrieve the demanded torque from the look-up tables shown in Fig. 6. Once the control look-up values are read,

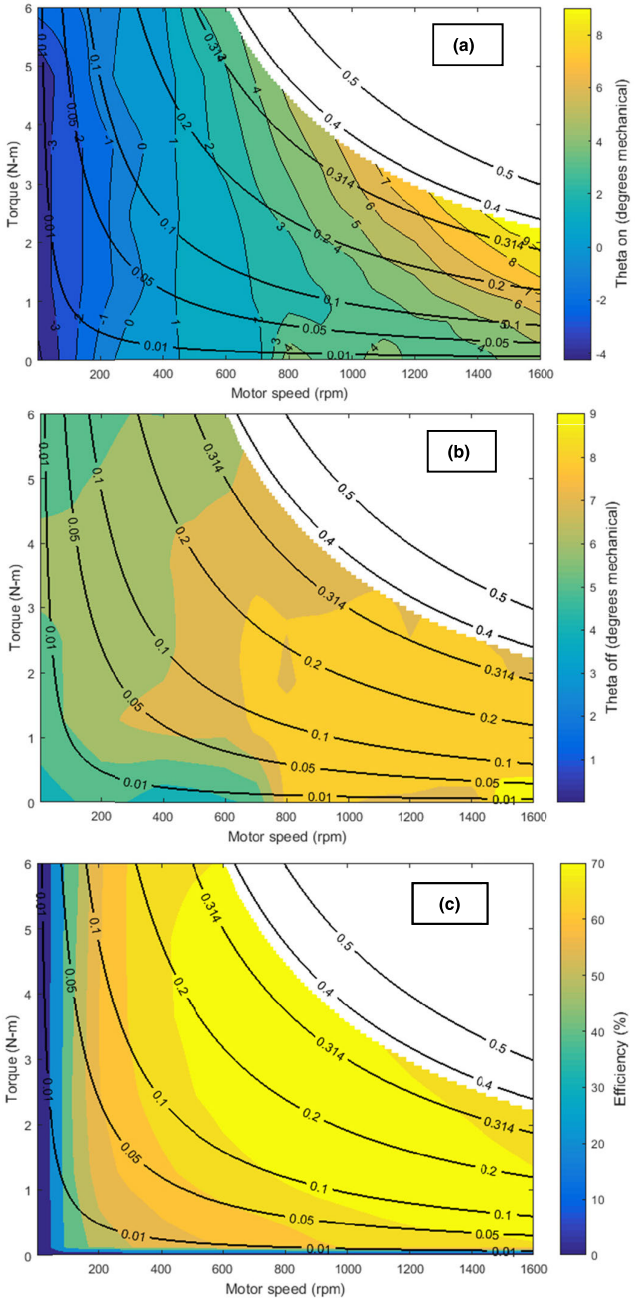


**FIGURE 6.** (a) SR machine phase turn on angle look-up table as a function of torque and speed demand, including the selected constant mechanical power curves (kW) as functions of the speed. (b) Turn off angle look-up table as a function of torque and speed demand. (c) SR machine efficiencies look-up table as a function of torque and speed demand, including the selected constant mechanical power curves (kW) as functions of speed. Mechanical power is calculated from torque and speed. For these analyses the zero-degree angle is where the poles are fully aligned.

the switching signals $s_i$ are used to switch the phase currents in the half-bridge converter. SRM is designed to respond to the human pedaling torque change if the required signals are updated at a sub-second time interval (e.g. the bandwidth is 100Hz).

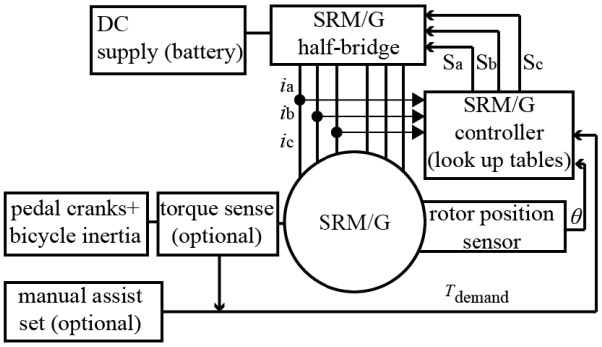


**FIGURE 7.** Schematic control of the SRM.

**TABLE 2.** Electrically assisted bicycle model parameters.

| Parameter | Quantity |
|---|---|
| Mass of e-bike and cyclist (M) | 100 (kg) |
| Bicycle wheel rolling radius(R) | 0.33 (m) |
| Gravitational constant (g) | 9.81 (m/s$^2$) |
| Density of air ($\rho$) | 1.23 (kg/m$^3$) |
| Aerodynamic drag coefficient ($C_d$) | 0.5 |
| Frontal area, $A$ | 0.5 (m$^2$) |
| Tire rolling resistance coefficient ($\mu_{rr}$) | 0.004 |
| Road gradient ($\theta$) | 0 (degrees) |
| Maximum cadence per minute[1] | 120 (cpm) |
| On board battery voltage (V) | 45 (Volt) |
| On board battery current (A) | 40 (Apeak) |
| Bicycle gearing ratio ($BG_r$) | 3 |
| Electric motor gearing ratio ($G_r$) | 13 |

[1]Assuming average cyclist performance capabilities [28]

## IV. BICYCLE DYNAMICS WITH THE ONBOARD SRM

### A. ANALYSIS OF THE BICYCLE DYNAMICS

This section analyses the complex dynamic system, which arises due to the synergetic combination of the cyclist and electric motor torques, that vary dynamically over the complete pedal crank revolution (as in Fig. 2b). The case of the European urban driving cycle was chosen as an exemplar [37], with a total duration of 190 seconds, and a distance of 0.513 kilometers on a level road. The driving schedule does not exhibit demanding acceleration and velocity profiles as would be expected from cars, making it suitable for the dynamic performance simulation and evaluation of the proposed human-electric bicycle combination [6]. This driving cycle schedule will be completed by the two assistance torque modes in exactly the same time to facilitate comparison. To create a common benchmark, the same model parameters defined for the bicycle [6], as listed in Table 2 were used. This study assumes the motor is situated on the pedal crank case via the gearing in a mid-crank type arrangement.

Using the published model bicycle parameters from Table 2, together with the chosen driving schedule, the

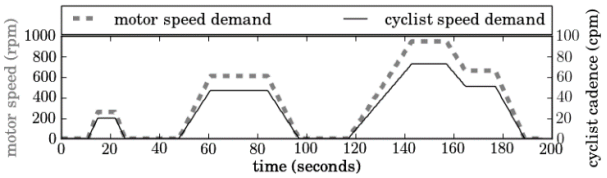


**FIGURE 8.** Cyclist cadence rate and motor rotational speed demand according to the urban cycling schedule [37] and the model parameters from Table 2.

speed-torque demand for the bicycle propulsion is [38]

$$\frac{G}{R}T = \mu_{rr}Mg + \frac{1}{2}\rho AC_d v^2 + \left(M + J\frac{G}{\eta R^2}\right)\frac{dv}{dt}, \quad (6)$$

where $J$ is the total system inertia, $\eta$ is the gearing efficiency, and where the bicycle velocity $v$ is taken directly from the known driving schedule speed profile (Fig. 8) for the bicycle speed demand. Equation 6 enables torque demand computation at each time step of the chosen urban cycling schedule of Fig. 8 with the resulting corresponding torque demand as in Fig. 9. The two figures contain the speed and torque demand signals that would be required for the human only or electric motor only cases, for the chosen motor gearing ratio of 13. The motor rotational speed is exactly 13 times higher and follows the cyclist cadence rate (cadence: rotation per minute) as in Fig. 8. In Fig. 9 the required cyclist-only propulsion torque is slightly lower than the motor-only torque since the motor gearing will inevitably introduce some mechanical inefficiency. The simulated driving schedule torque demand results in Fig. 9 indicate that the highest demanded signals coincide with the periods of the bicycle acceleration in Fig. 8, where the speed rise is achieved in a short time period. Further, the driving schedule torque demand is reduced as the steady speed is achieved and maintained by the bicycle. Nevertheless, whatever the chosen bicycle propulsion torque source; human, electric or the combination of the two, the highest torque demand will occur with the greatest acceleration demand. This corresponding maximum torque demand will in turn define the required torque rating of the SRM. Fig. 10 shows such speed-torque demand from the motor at each time step of the simulated urban cycling schedule. By superimposing the results from Fig. 9 onto Fig. 6c, the designed SR machine demonstrably delivers on the required speed-torque demand for the cycling schedule on its own as shown in Fig. 10.

Furthermore, Fig. 10 contains the demanded torque points of the modelled driving schedule in Fig. 9 showing the difference between the assistive constant torque mode (+ sign) and the modulated sinusoidally varying torque mode (o sign). The modulated torque points are shown in pairs where lower points (red) are the troughs of the sinusoidal torque wave and the upper points (blue) are the peaks of the same curve. It should be understood that; although the operating torque points do not reach even half of the maximum torque capability of the designed SRM this is the case since

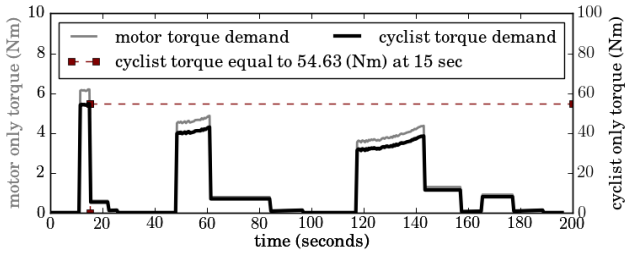


**FIGURE 9.** Bicycle propulsion torque demand according to the urban cycling schedule [37] and the model parameters from Table 2 and Eq. (6).

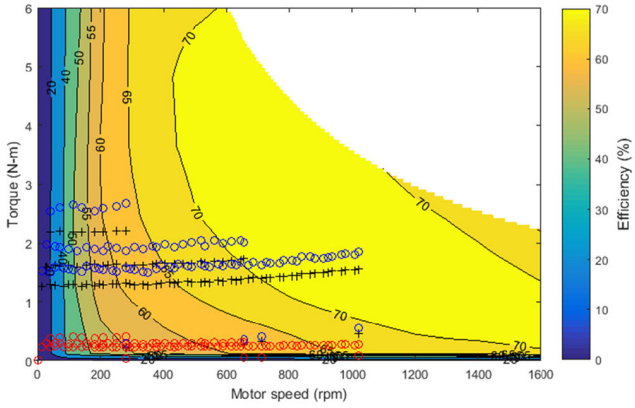


**FIGURE 10.** Constant motor torque demand (+ sign) and modulated motor torque demand (o sign) for the urban cycling schedule as a function of the motor speed. The lines in the graph indicate the efficiency values.

the chosen driving schedule is a simple representative real world profile. Therefore, the designed SR machine should have much higher torque capacity in order to accommodate more demanding cycling profiles required by real world conditions.

### *B. HUMAN CYCLING TORQUE PRODUCTION*

Given that the designed SRM speed-torque performance is completely described by the look-up tables, it becomes necessary to construct a similar look-up map of the speed-torque for the cyclist. Fig. 11 shows this map, and assumes that in addition to the cyclist's sinusoidally varying instantaneous torque, the cadence of the cyclist is of considerable importance when attempting to deliver the specific torque demand. Specifically, as is found in the experimental investigations involving cyclists [28], and specified in Table 2, the measured maximum attainable cadence is 120 revolutions per minute.

A faster cadence is possible, but only in athlete cyclists. Despite this, if the cyclist is cycling at this maximum specified cadence rate, the torque output is reduced to zero following the parabolically varying propulsion power production law [28]. Therefore, at the highest cycling rate in the presence of the pedaling motion there is no useful cycling propulsion torque production. Furthermore, the maximum instantaneous cycling torque scales linearly with cadence, so instantaneous torque reaches its maximum at zero cadence.

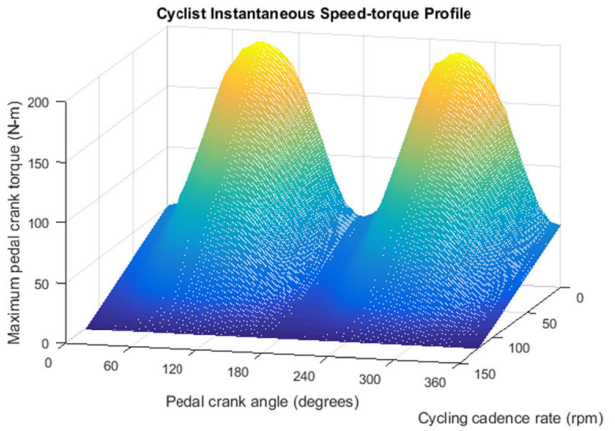


**FIGURE 11.** Model instantaneous cyclist torque as a function of the crank angle and cadence rate, assumed to decrease linearly with the increase in cadence rate [28].

**TABLE 3.** Energy expenditure for the constant and modulated case.

| Energy expenditure mode (Energy in Joules) | Cycling schedule | Cycling schedule + 1/40 gradient | Cycling schedule + 1/40 gradient + 20% headwind |
|---|---|---|---|
| Total constant energy | 11277.7 | 25263.9 | 26204.4 |
| Constant motor energy | 7208.7 | 15885.1 | 16464.5 |
| Constant cyclist energy | 4069 | 9378.8 | 9740 |
| Total modulated energy | 11462.8 | 25113.3 | 26012.4 |
| Modulated motor energy | 7407.6 | 16001.1 | 16554.5 |
| Modulated cyclist energy | 4055.2 | 9112.2 | 9458 |

Based on Fig. 11, the cyclist can choose to regulate the instantaneous output torque at each cadence rate to adjust to the demanded cycling torque.

### *C. SYNERGETIC HUMAN AND MOTOR TORQUE COMBINATION*

Once the motor and human propulsive torque models are defined, they are combined to form the total propulsive torque as discussed in section 2.2 and shown in Fig. 2b. For example; in order to extract the sinusoidally varying instantaneous propulsive torque demand from Fig. 11 at a particular cadence rate of the cyclist it is necessary to vary the motor torque in such a way that the motor torque completely fills the troughs (dips) of the human torque so as to maintain the originally demanded total propulsion torque in Fig. 9. In other words; the sinusoidal output torque control of the motor follows the sinusoidal torque reference signal which is phase offset from the cyclist torque signal. This requirement is fulfilled instantaneously by the designed SRM at each pedal crank angle as shown in Fig. 12.

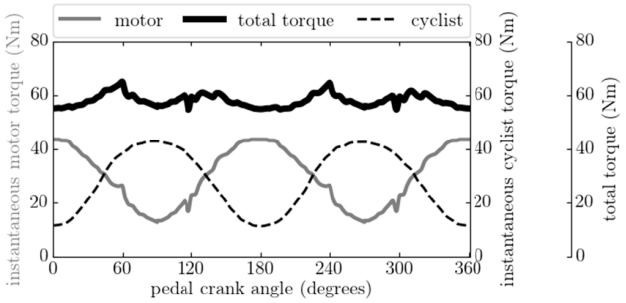


**FIGURE 12.** Instantaneous human torque, average instantaneous motor torque, and the synergetic total propulsion torque of those two sources.

The instant shown in Fig. 12 is at 15 seconds into the cycling schedule of Fig. 9 at a modest cadence of twenty revolutions per minute. The demanded motor speed at this instant is 260 (rpm) due to the gearing ratio of 13. The total demanded average propulsion torque at this instant is 54.63 (Nm) (i.e. an operating point of 2.5 Nm at 260 rpm in Fig. 10). It can be deduced by visual inspection of Fig. 9 that the delivered cyclist torque at the chosen instant is only half of the total demanded propulsive torque, since the other half is delivered by the motor. Figure 12 confirms that the averaged sinusoidal motor torque contributes exactly half the demanded propulsion torque, as suggested in Fig. 2b, and that the highest instantaneous assistive torque is delivered exactly at the least effective pedal crank angles (as depicted in Fig. 1).

### D. SYNERGETIC ASSISTIVE TORQUE ENERGY SAVINGS

To investigate electrical energy savings from the synergetic combination of the human and the SRM torques, the cycling schedule shown in Fig. 8 was repeated for the two torque assistance modes. The first motor assistance case was where exactly half of the demanded propulsion torque was delivered by the SRM following a constant torque demand signal (motor 1) as in Fig. 2a. The second motor assistance case was configured to deliver exactly half the demanded propulsion torque with the SRM assistive torque following the instantaneously varying human torque signal as in Fig. 2b. The cycling schedule of Fig. 8 was run once for each case using the model parameters of Table 2 in order to compare these cases.

Table 3 presents the obtained results comparisons. Cyclist energy expenditure in both assistive cases is practically the same, indicating that the cyclist is indifferent to the motor torque assistive mode. This result confirms the proposition that the two motor torque assistance schemes in Fig. 2 are equivalent as far as human energy input is concerned. Comparison of the motor electric energy expenditure for the sinusoidally modulated instantaneous torque and the constant motor torque assistance mode, for the chosen cycling schedule, reveals that the two assistance modes are equivalent and consume the same amount of energy (to within a 2% difference at most among the considered cycling schedules), as detailed in Table 3. Alternatively, the energy expenditure

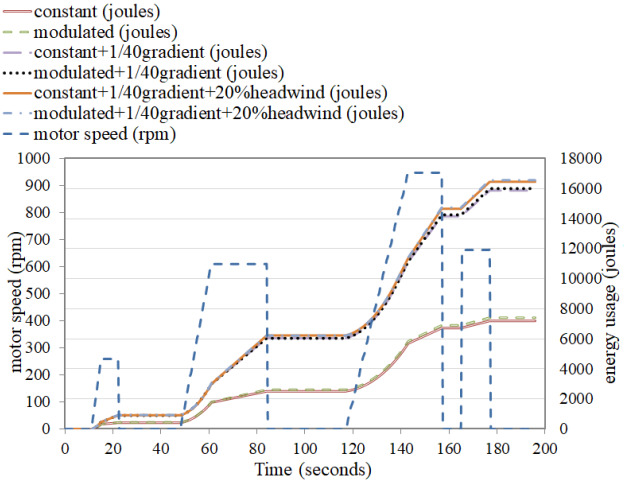


**FIGURE 13.** Motoring energy expenditure as a function of the cycling schedule for the constant torque and modulated torque modes.

progression for the two assistive motor cases can be visualized against the cycling schedule of Fig. 8, that which represents the cycling journey of less than 4 minutes and 0.513 km, as in Fig. 13.

The energy expenditure in Fig. 13 has been calculated by taking each cycling profile point, the demanded torque at the demanded speed, and looking-up this set of values in the efficiency map in Fig. 6c and dividing the torque × speed value by the efficiency value at that point and integrating it in time in order to get the total energy required. Therefore this calculation accounts for all the machine losses including the copper losses.

Figure 13 indicates the cumulative increase in motor electrical energy expenditure in time. This figure shows that, if the demanded acceleration of the bicycle is low, the energy consumption of the motor is also low. On the other hand, once the bicycle acceleration demand is increased to a modest level, for example at the 120 seconds mark into the schedule of Fig. 8, the energy expenditure of a motor increases significantly.

The comparison of the actual energy expenditure of the two torque assistance modes in Fig. 13 confirms that the two torque modes also consume practically equal amount of electrical energy. This result is counterintuitive from the first sight since it is understood that in order to generate a higher-than-average torque level, a level which occurs when the motor is operated with the sinusoidally varying torque mode, the electric current supplied into the motor will have to be proportionally higher compared to the constant torque motor current. This result is shown in Fig. 14 corresponding to the specific motor operating conditions in Fig. 12.

However, Fig. 14 also shows that, in addition to operating at a significantly higher current level in the sinusoidally varying torque mode, the same motor operates at a significantly lower current level exactly half of the time. Consequently, the total electric energy expenditure for the sinusoidally

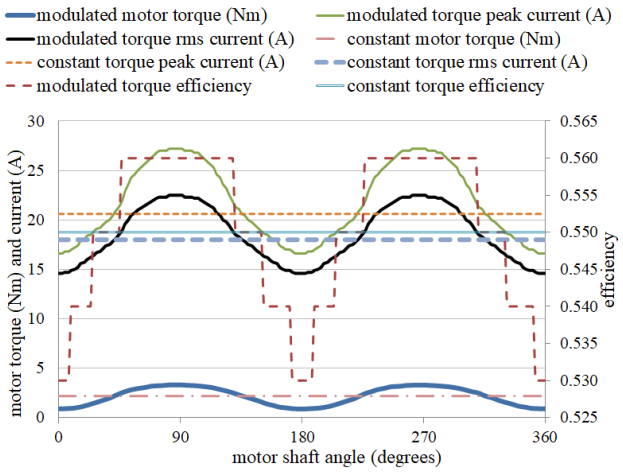


**FIGURE 14.** Phase currents and motor efficiencies as functions of the cyclist instantaneous torque for the constant and the modulated torque modes.

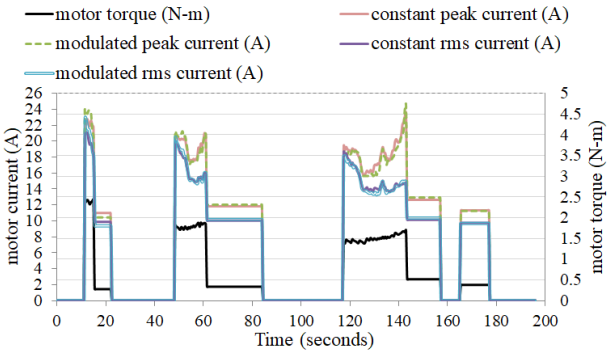


**FIGURE 15.** Constant and modulated motor phase currents as functions of the cycling schedule.

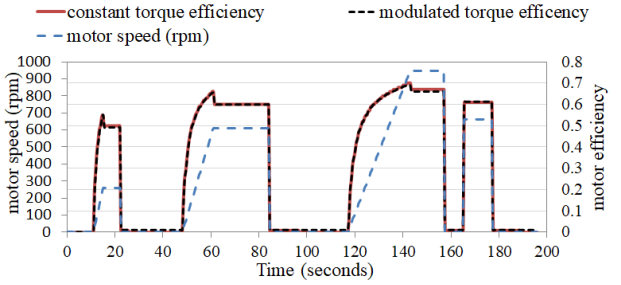


**FIGURE 16.** Constant and modulated motor efficiencies as functions of the cycling schedule.

operated motor is the same as that of the motor operating in the constant torque mode. Therefore, the sinusoidal torque control mode can be considered to be more advantageous compared to the constant torque control mode since the two torque modes deliver equal average torque levels and thus the cycling performance for a given cycling schedule is not affected.

However, by using the sinusoidal torque assistance the cyclist is encouraged to cycle in the most natural cycling mode and posture [23]–[30], [32], as would occur if motor assistance was completely absent, since the sinusoidal assistance torque is delivered precisely at the least effective human torque points as discussed in Fig. 1. This suggests a possible broader application area as well, beyond everyday cycling, and could include physical rehabilitation exercise ergometers.

The results in Table 3 and Fig. 13 are encouraging since, if it is possible to achieve the same energy expenditure level with the sinusoidal torque control mode over the very short cycling route of less than 4 minutes and without any assumed uphill cycling, then for more challenging and longer cycling routes, the required cyclist energy input should not be adversely affected by the use of the modulated torque motor.

The effects of a 1:40 increase of the road gradient (Fig. 13) show that the energy expenditure of the modulated assistive torque mode is practically equal to the constant assistive torque mode on this incline. If the considered cycling schedule, in addition to the added road incline, is now assumed to be subject to an additional 20% head wind resistance, the two motor torque assistance modes are indifferent in terms of performance and the energy expenditure since the energy expenditure of the compared motor modes are practically equal. These results are compared in Table 3 and Fig. 13. These results can be further confirmed in Fig. 15 and Fig. 16 showing the comparisons of the electric currents and the efficiencies for the two motor assistance modes.

The proceeding results show that, if the motor torque is modulated with the human instantaneous torque profile, the modulated motor power rating could be reduced as the duty cycle is reduced. This in turn would require a smaller SR machine. This results in significant savings in terms of production materials requirement for the high volume electric bicycle manufacture.

## V. CONCLUSION

A novel electric motor torque control mode for bicycles equipped with a switched reluctance motor is proposed. Cyclists are a rich source of kinetic energy; however, when applying propulsive energy conversion technology of conventional cycling, it is important to minimize the increase in extra muscular activity and to maximize the efficiency of the conversion. To achieve this, and to reduce the torque demand, a modulated torque motor has been proposed. Comparisons of the two motor control modes presented in this article show that a motor with a sinusoidally modulated torque consumes an equal amount of the electric energy compared to a motor with a constant torque over a cyclist's journey. Practical torque measurement techniques and signal conditioning should be considered in order to implement the modulating torque in practice. In this article no attempt was made to design a particular bicycle.

The results from this analysis suggest a further investigation into the effectiveness of the energy harvesting, as well as modulated motor torque assistance in electrically assisted bicycling. Further investigations are planned whereby a

prototype SR machine is built and experimentally tested for the considered cycling schedules and torque control modes in order to confirm the theoretical simulations presented in this work and to investigate potential energy savings with the use of specifically optimized motor control look-up tables.

## REFERENCES

[1] S. Cairns, F. Behrendt, D. Raffo, C. Beaumont, and C. Kiefer, "Electrically-assisted bikes: Potential impacts on travel behaviour," *Transp. Res. A, Policy Pract.*, vol. 103, pp. 327–342, Sep. 2017.
[2] W. Chlebosz, G. Ombach, and J. Junak, "Comparison of permanent magnet brushless motor with outer and inner rotor used in e-bike," in *Proc. 19th Int. Conf. Electr. Mach. (ICEM)*, Sep. 2010, pp. 1–5.
[3] E. Starschich and A. Muetze, "Operating area analysis of direct and geared brushless-DC motor drives for electric bicycles," in *Proc. IEEE Ind. Appl. Annu. Meeting*, Sep. 2007, pp. 2161–2168.
[4] Y. Yang, M. M. Rahman, T. Lambert, B. Bilgin, and A. Emadi, "Development of an external rotor V-shape permanent magnet machine for E-bike application," *IEEE Trans. Energy Convers.*, vol. 33, no. 4, pp. 1650–1658, Dec. 2018.
[5] E. Starschich and A. Muetze, "Comparison of the performances of different geared brushless-DC motor drives for electric bicycles," in *Proc. IEEE Int. Electr. Mach. Drives Conf.*, vol. 1, May 2007, pp. 140–147.
[6] J. Lin, N. Schofield, and A. Emadi, "External-rotor 6–10 switched reluctance motor for an electric bicycle," *IEEE Trans. Transport. Electrific.*, vol. 1, no. 4, pp. 348–356, Dec. 2015.
[7] L. I. Jusoh, E. Sulaiman, F. S. Bahrim, and R. Kumar, "Design comparison of inner and outer rotor of permanent magnet flux switching machine for electric bicycle application," *IOP Conf. Ser., Mater. Sci. Eng.*, vol. 226, Aug. 2017, Art. no. 012129.
[8] R. A. Inte and F. N. Jurca, "A novel synchronous reluctance motor with outer rotor for an electric bike," in *Proc. Int. Conf. Expo. Electr. Power Eng. (EPE)*, Oct. 2016, pp. 213–218.
[9] M. Z. Islam and S. Choi, "Design of rare-earth free five-phase outer-rotor IPM motor drive for electric bicycle," in *Proc. IEEE Appl. Power Electron. Conf. Expo. (APEC)*, Mar. 2016, pp. 631–637.
[10] B. Y. A. Muetze and Y. C. Tan, "Electric bicycles: A performance evaluation," *IEEE Ind. Appl. Mag.*, vol. 13, no. 4, pp. 12–21, Jul. 2007.
[11] K. Fujii, H. Kumai, E. Ishii, S. Higaki, S. Yamaguchi, and H.-A. Zhao, "Researches on small capacity vehicles driven by induction machine," in *Proc. 6th Int. Workshop Adv. Motion Control*, Nagoya, Japan, 2000, pp. 465–468, doi: 10.1109/AMC.2000.862916.
[12] E. Bostanci, M. Moallem, A. Parsapour, and B. Fahimi, "Opportunities and challenges of switched reluctance motor drives for electric propulsion: A comparative study," *IEEE Trans. Transport. Electrific.*, vol. 3, no. 1, pp. 58–75, Mar. 2017, doi: 10.1109/TTE.2017.2649883.
[13] C. Gan, J. Wu, Q. Sun, W. Kong, H. Li, and Y. Hu, "A review on machine topologies and control techniques for low-noise switched reluctance motors in electric vehicle applications," *IEEE Access*, vol. 6, pp. 31430–31443, 2018.
[14] B. Fahimi, A. Emadi, and R. B. Sepe, "A switched reluctance machine-based starter/alternator for more electric cars," *IEEE Trans. Energy Convers.*, vol. 19, no. 1, pp. 116–124, Mar. 2004.
[15] H. A. Chen, X. Me, and J. Jiang, "The switched reluctance motor drive for application in electric bicycle," in *Proc. IEEE Int. Symp. Ind. Electron. (ISIE)*, vol. 2, Jun. 2011, pp. 1152–1156.
[16] B. Kerdsup and N. H. Fuengwarodsakul, "Performance and cost comparison of reluctance motors used for electric bicycles," *Electr. Eng.*, vol. 99, no. 2, pp. 475–486, Jun. 2017.
[17] R. Gabor, M. Kowol, J. Kolodziej, and P. Mynarek, "Steady state analysis of switched reluctance motor with modified geometry of the stator designed for an electric bike," in *Proc. Int. Symp. Electr. Mach. (SME)*, Andrychów, Poland, Jun. 2018, pp. 1–5.
[18] M. A. Khan, F. Khan, U. Jamshed, S. Ali, Z. Ajmal, A. Zahid, and N. Ahmad, "Design and analysis of outer segmental rotor synchronous reluctance machine for future electric bike," in *Proc. Int. Conf. Eng. Emerg. Technol. (ICEET)*, Lahore, Pakistan, Feb. 2019, pp. 1–5.
[19] J. W. Jiang, B. Bilgin, B. Howey, and A. Emadi, "Design optimization of switched reluctance machine using genetic algorithm," in *Proc. IEEE Int. Electr. Mach. Drives Conf. (IEMDC)*, Coeur d'Alene, ID, USA, May 2015, pp. 1671–1677, doi: 10.1109/IEMDC.2015.7409288.
[20] B. Howey, "Non-coupled and mutually coupled switched reluctance machines for an E-bike traction application: Pole configurations, design, and comparison," Ph.D. dissertation, Dept. Mech. Eng., McMaster Univ., Hamilton, ON, Canada, 2018.
[21] M. V. de Paula, T. A. dos Santos Barros, and P. J. Neto, "A review of classic torque control techniques for switched reluctance motors," in *Modelling and Control of Switched Reluctance Machines*. London, U.K.: IntechOpen, 2020, doi: 10.5772/intechopen.89450.
[22] A. Stuikys, B. Zaghari, and J. K. Sykulski, "Instantaneous electromagnetic torque waveform calculations for switched reluctance machines exploiting vector analysis," *IEEE Trans. Magn.*, early access, Oct. 28, 2020, doi: 10.1109/TMAG.2020.3034565.
[23] T. Rowe, M. L. Hull, and E. L. Wang, "A pedal dynamometer for off-road bicycling," *J. Biomech. Eng.*, vol. 120, no. 1, pp. 160–164, Feb. 1998.
[24] R. R. Neptune and M. L. Hull, "Evaluation of performance criteria for simulation of submaximal steady-state cycling using a forward dynamic model," *J. Biomech. Eng.*, vol. 120, no. 3, p. 334, 1998.
[25] R. R. Bini, P. A. Hume, J. Croft, and A. E. Kilding, "Pedal force effectiveness in cycling: A review of constraints and training effects," *J. Sci. Cycl.*, vol. 2, no. 1, pp. 11–24, 2013.
[26] G. E. Caldwell, L. Li, S. D. McCole, and J. M. Hagberg, "Pedal and crank kinetics in uphill cycling," *J. Appl. Biomech.*, vol. 14, no. 3, pp. 245–259, Aug. 1998.
[27] T. Korff, L. M. Romer, I. Mayhew, and J. C. Martin, "Effect of pedaling technique on mechanical effectiveness and efficiency in cyclists," *Med. Sci. Sports Exerc.*, vol. 39, no. 6, pp. 991–995, Jun. 2007.
[28] F. R. Whitt, D. G. Wilson, and J. Papadopoulos, *Bicycling Science*. Cambridge, MA, USA: MIT Press, 2004.
[29] J. Newmiller, M. L. Hull, and F. E. Zajac, "A mechanically decoupled two force component bicycle pedal dynamometer," *J. Biomech.*, vol. 21, no. 5, pp. 375–386, Jan. 1988.
[30] C. Outram, C. Ratti, and A. Biderman, "The Copenhagen Wheel: An innovative electric bicycle system that harness the power of real-time information and crowd sourcing," in *Proc. EVER Monaco, Conf. Ecol. Vehicles Renew. Energies*, 2010.
[31] *Motor Assisted Cycle Regulation*, B.C. Reg. 151/2002 Insurance Corp. British Columbia, North Vancouver, BC, Canada, 2018.
[32] A. Fuchs, "Principles of human-electric hybrid drives for human powered vehicles," in *Proc. Semin. Eur. Copenhagen, Velomobile Des.*, 2009, pp. 1–24.
[33] M. Takeno, A. Chiba, N. Hoshi, S. Ogasawara, M. Takemoto, and M. A. Rahman, "Test results and torque improvement of the 50-kW switched reluctance motor designed for hybrid electric vehicles," *IEEE Trans. Ind. Appl.*, vol. 48, no. 4, pp. 1327–1334, Jul. 2012.
[34] A. Stuikys and J. Sykulski, "Rapid multi-objective design optimisation of switched reluctance motors exploiting magnetic flux tubes," *IET Sci., Meas. Technol.*, vol. 12, no. 2, pp. 223–229, Mar. 2018.
[35] *MagNet Software*. Accessed: Jan. 15, 2020. [Online]. Available: http://www.mentor.com
[36] D. C. Meeker. *Finite Element Method Magnetics (FEMM), Version 4.2 (28Feb2018 Build)*. Accessed: Sep. 10, 2020. [Online]. Available: http://www.femm.info
[37] D. M. Sousa, P. J. C. Branco, and J. A. Dente, "Electric bicycle using batteries and supercapacitors," in *Proc. Eur. Conf. Power Electron. Appl. (EPE)*, 2007, pp. 1–10.
[38] W. C. Morchin and H. Oman, *Electric Bicycles: A Guide to Design and Use*. Hoboken, NJ, USA: Wiley, 2006.

**BAHAREH ZAGHARI** (Member, IEEE) received the M.Sc. degree (Hons.) in advanced mechanical engineering (mechatronics) from the University of Southampton, U.K., in 2012, and the Ph.D. degree in dynamic analysis of a nonlinear parametrically excited system using electromagnets from the Institute of Sound and Vibration (ISVR), University of Southampton, in 2017. She was a Research Fellow with the School of Electronics and Computer Science, where she has been working on the design of smart systems, such as the next generation of jet engines and smart cities. She is currently a Lecturer in propulsion integration with Canfield University and a Visiting Fellow with the University of Southampton. She has received several awards for her outstanding performance in supporting women in academia.

**ALEKSAS STUIKYS** received the B.Sc. degree in mechanical engineering and the M.Sc. degree in advanced engineering design from Oxford Brookes University, Oxford, U.K., in 2009 and 2011, respectively, and the Ph.D. degree from the School of Electronics and Computer Science, Institute for Complex Systems Simulation, University of Southampton, Southampton, U.K., in 2018.

He is currently the Founder of RETORQ Motors Ltd., company specializing in the advanced electric traction motor and propulsion systems technology research and development for the electrification of transportation. His research interests include propulsion systems, including electric traction motors; their modeling, simulation, and design for the electric and hybrid vehicles and for the sustainable transport in general. His research interest also includes the modeling, design, and control aspects of switched reluctance machines-based traction systems.

**ALEX S. WEDDELL** (Member, IEEE) received the M.Eng. (Hons.) and Ph.D. degrees in electronic engineering from the University of Southampton, U.K., in 2005 and 2010, respectively. He is currently a Lecturer with the Center for Internet of Things and Pervasive Systems, University of Southampton, and is involved with three projects funded by EPSRC, EU Horizon 2020, and Clean Sky 2. His main research interests include energy harvesting and energy management for the future Internet of Things devices. He has over 14 years of experience in design and deployment of energy harvesting systems, and has published around 55 peer-reviewed articles in the area.

**STEVE BEEBY** (Senior Member, IEEE) received the B.Eng. (Hons.) degree in mechanical engineering from the University of Portsmouth, Portsmouth, U.K., in 1992, and the Ph.D. degree in MEMS resonant sensors from the University of Southampton, Southampton, U.K., in 1998. He was a Principal or a Co-Investigator on an additional 18 projects and has coordinated two European Union research projects. He is currently the Head of the Smart Electronic Materials and Systems Research Group. He leads the U.K.'s Energy Harvesting Network. He is currently leading three U.K. funded research projects. He is the Co-Founder of Perpetuum Ltd., a University spin-out based upon vibration energy harvesting formed in 2004, Smart Fabric Inks Ltd., and D4 Technology Ltd. He has coauthored/edited four books, including *Energy Harvesting for Autonomous Systems* (Artech House, 2010). He has given 17 invited talks and has over 250 publications and ten patents. He has an H-index of 50. His current research interests include energy harvesting, e-textiles, MEMS, and active printed materials development. He was a recipient of two prestigious EPSRC Research Fellowships to investigate the combination of screen-printed active materials with micromachined structures and textiles for energy harvesting and was also awarded the Personal Chair in 2011.